Capture of hot holes by shallow acceptors in *p*-type GaAs studied by picosecond infrared spectroscopy

M. Woerner, A. Lohner, T. Elsaesser, and W. Kaiser
Physik Department E 11, Technische Universität München, D-8046 Garching, Federal Republic of Germany
(Received 25 September 1992)

Picosecond recombination of free holes with shallow acceptors in *p*-doped GaAs is directly monitored via spectrally and temporally resolved infrared studies. Neutral Zn impurities are photoionized by picosecond excitation in the wavelength range around 5 μm. The recombination dynamics of the free carriers with ionized acceptors is measured via transient changes of the acceptor deionization band at photon energies close to the band gap. Hole capture is observed on a time scale of up to 100 ps following nonexponential kinetics. The data are analyzed with the help of model calculations considering single-step as well as multiple-step trapping mechanisms. Emission of single longitudinal-optical phonons is found to be the main mechanism of picosecond recombination.

I. INTRODUCTION

Capture of free carriers and ionization of shallow impurities in extrinsic semiconductors are fundamental scattering processes between the continuum of the valence or conduction bands and levels localized at the impurity atoms. These transitions establish the respective equilibrium population of free and bound states at low temperatures and/or high doping concentrations, where a certain fraction of impurities are ionized. The same mechanisms are relevant for the nonequilibrium dynamics of optical transitions between delocalized and bound states such as band-to-acceptor luminescence[1] and for charge transport at high electric fields.[2] Repeated trapping and ionization processes, involving the excited states of the impurity atoms, reduce the conductivity of the material and lead to generation-recombination noise in semiconductor devices.[3,4]

Experimental studies have concentrated on stationary transport or electrical noise measurements giving capture cross sections for shallow donors and acceptors in silicon and germanium.[5,6] Much less information exists on the *microscopic dynamics* of carrier capture. Nanosecond trapping times have been deduced from time-resolved transport experiments on *n*-type germanium[7] and from the photo Hall effect of *p*-type silicon.[8] In GaAs, time-resolved studies of impurity-related luminescence report electron and hole capture on a time scale between 10 and 500 ns.[9] The observed relaxation rates are mainly determined by the interaction between free carriers of low kinetic energy and acoustic phonons.[2]

The experimental results have been analyzed with cascade capture models, where trapping is described as a sequence of scattering events by which the free carrier is transferred from the continuum to high-lying impurity states.[10] The amount of energy exchanged per scattering event has a small value of several meV and—correspondingly—cascade processes are dominated by carrier-carrier scattering and by emission of acoustic phonons. Detailed theoretical models have been developed to account for multiple scattering and to calculate cross sections of carrier capture.[2] Recently, Monte Carlo techniques have been applied to simulate the kinetics of charge transport.[2,11]

In many cases, the energy separation of the impurity ground state from the first excited state is significantly larger than the amount of energy transferred per carrier-carrier or carrier–acoustic-phonon collision. As a result, repopulation of the impurity ground state requires a final relaxation step with larger energy transfer. Radiative transitions, Auger processes, and emission of optical phonons[12] have to be considered as mechanisms relevant for this single-step relaxation.[13,14] In III-V semiconductors like GaAs, the interaction of free carriers with optical phonons is strong and enhanced capture rates are expected to occur if electrons and holes have sufficient energy to emit longitudinal- (LO) or transversal- (TO) optical phonons. The large energy of LO and TO phonons compared to acoustic phonons allows a direct transition from the continuum to the impurity ground state by emission of a single (optical) phonon if the phonon energy is higher than the ionization energy E_{acc} of the impurity. This process facilitates the effective capture of high-energy (i.e., hot) carriers and should—due to the strong carrier-phonon coupling—occur on a very fast time scale. Very recently, we have presented the first direct evidence of ultrafast capture of hot holes by shallow impurities in *p*-type GaAs.[15] We observed a nonexponential kinetics of trapping on a time scale of several 10^{-11} s^{-1} which was monitored by picosecond changes of the acceptor deionization band.

In this paper we present a more detailed study of hot hole trapping in GaAs using picosecond infrared pulses. The carrier dynamics is studied for different doping concentrations of the *p*-type crystals as well as for different lattice temperatures between 10 and 70 K. In addition, the absolute strength of the deionization band is determined both experimentally and by calculations of the absorption cross section extending the earlier treatment of Ref. 1. The time-resolved data are analyzed by detailed

theoretical simulations considering several single- and multiple-step mechanisms of carrier capture. Emission of single longitudinal-optical phonons is found to be the dominant capture mechanism for direct population of the acceptor ground state.

The paper is organized as follows. After a brief description of the experimental technique in Sec. II, the experimental results are presented in Sec. III. Section IV gives a qualitative discussion of the relaxation processes initiated by photoexcitation in the infrared. In Sec. V, we quantitatively calculate the acceptor deionization band. The different trapping mechanisms are discussed in Sec. VI and the relevant capture rates are calculated and compared with the data. Finally, our results are summarized.

II. EXPERIMENT

In our experiments we investigate two Zn-doped GaAs crystals with respective acceptor concentrations of $N_A = 7\times10^{17}$ and 2.3×10^{17} cm^{-3}. The samples which are glued on BaF_2 substrates have a thickness of $l \simeq 10^{-3}$ cm. The crystals are attached to the cold finger of a closed-cycle helium cooler allowing the variation of the sample temperature between 10 and 300 K.

The schematic band structure of p-type GaAs in Fig. 1

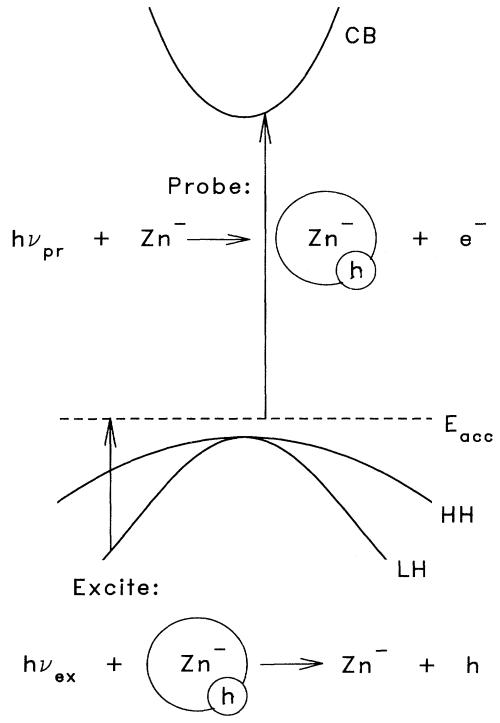

FIG. 1. Schematic of the band structure of p-type GaAs indicating the experimental technique used in the time-resolved measurements. Intense infrared pulses photoionize the neutral Zn acceptors A^0 by promoting electrons e^- from the light-hole (LH) band to the aceptor ground state. In this way, free holes are created which are subsequently trapped by the A^- ions. The momentary occupation of the acceptor ground state E_{acc} is monitored via the transient deionization band. The arrows mark transitions of electrons.

illustrates the excitation and probe scheme of our time-resolved experiment in an electron picture. The acceptor ground state is marked by the dashed line. At low lattice temperatures $k_B T_L \ll E_{acc} \simeq 30$ meV (Ref. 16) (E_{acc}: acceptor ionization energy), the acceptors are neutral (A^0), corresponding to holes bound at the impurity atoms. An intense infrared pulse excites electrons from the light-hole band (LH) to the acceptor ground state: $h\nu_{ex} + e^- + A^0 \rightarrow A^-$, resulting in ionized, negatively charged acceptor atoms and *free* holes in the light-hole band which subsequently redistribute among different valence-band states. Probe photons with an energy close to the fundamental band gap promote electrons e^- to the conduction band (CB): $h\nu_{pr} + A^- \rightarrow A^0 + e^-$. In the probing process the negative charge of the acceptors is canceled; thus the corresponding absorption band was named the acceptor deionization band.[17] Spectrally and time-resolved measurements of this transient absorption give direct information on the depopulation and repopulation of the acceptor ground-state levels, i.e., on the kinetics of free hole-acceptor recombination.

In our investigation, we need two well-synchronized picosecond pulses at substantially different wavelengths. Tunable excitation pulses in the wavelength range from 5 to 12 μm are generated by parametric frequency conversion. Pulses of a mode-locked Nd:glass laser and the output of a traveling-wave dye laser[18] working in the near infrared are mixed in a nonlinear $AgGaS_2$ crystal[19] to generate intense infrared pulses of 2 ps duration at the difference frequency. For the picosecond probing pulses, a white light continuum is generated by parametric four-photon interaction in water using the fundamental of the Nd:glass laser ($\lambda = 1.054$ μm) as pump pulse.[20] Probe pulses at the required spectral position near the band edge of GaAs are selected with interference filters providing a spectral resolution of 8 meV. The temporal resolution of the experiment has a value of 2 ps. The excitation density N_{ex} is estimated from the intensity of the pump pulse, the spot size, and the absorption coefficient of the respective sample at the photon energy of the pump giving values around $N_{ex} = 10^{17}$ cm^{-3}.

In addition to the pump-probe experiments, we studied the band-to-acceptor luminescence in steady state as well as time-resolved measurements. The stationary luminescence spectra and the quantum yield of the emission were determined with an $f = 25$ cm monochromator in conjunction with a calibrated Si photodiode. The spectral resolution was 2 meV. The luminescence decay times were measured with a single pulse streak camera system after picosecond excitation at 630 nm. The time resolution was 5 ps.

III. EXPERIMENTAL RESULTS

A. Stationary absorption and luminescence spectra

p-type GaAs exhibits strong absorption bands in the midinfrared spectral region.[21,22] At lattice temperatures $T_L > 200$ K and at low doping concentrations $N_A < 10^{17}$ cm^{-3}, the majority of acceptors is ionized and the in-

frared spectra are dominated by *direct* transitions of free holes between the different valence bands [heavy-hole (HH), light-hole, and split-off (SO) bands]. At low lattice temperatures $T_L < 100$ K, part of the holes are bound to the acceptor ions in hydrogenlike ground-state orbitals. Now, the infrared absorption below the fundamental band gap is governed by transitions of holes from these localized states to one of the three valence bands.[22] Figure 2(a) shows the stationary infrared absorption spectrum of the Zn-doped GaAs crystal with $N_A = 7\times10^{17}$ cm^{-3} at $T_L = 10$ K. The absorption coefficient is plotted on a logarithmic scale as a function of the infrared photon energy. The absorption between 350 and 500 meV is due to transitions of holes from the acceptor levels (acc.) to the splitoff band (acc.$\rightarrow$SO). In our experiments, the transition of bound holes to the light-hole band (acc.$\rightarrow$LH) located between 0.1 and 0.3 eV serves for (photo)generation of free holes. The photon energy of the infrared excitation pulses is marked by the arrow E_{ex}.

The near-infrared absorption (solid lines) and emission spectra (dashed lines) of the two samples are plotted in Figs. 2(b) and 2(c) for a lattice temperature of $T_L = 10$ K. The absorption edge is due to transitions from delocalized states in the valence band to the conduction band. In contrast, the luminescence spectra are dominated by recombination of free electrons with holes localized in the acceptor ground state [band-to-acceptor (BA) luminescence] whereas band-to-band recombination is negligible at this low temperature. Correspondingly, the luminescence spectrum peaks at $\Delta E \simeq 20$ to 30 meV below the fundamental band edge where ΔE is close to the acceptor binding energy. The bandwidth of the emission spectra ranges between 10 and 20 meV with a higher value for the higher doping density.

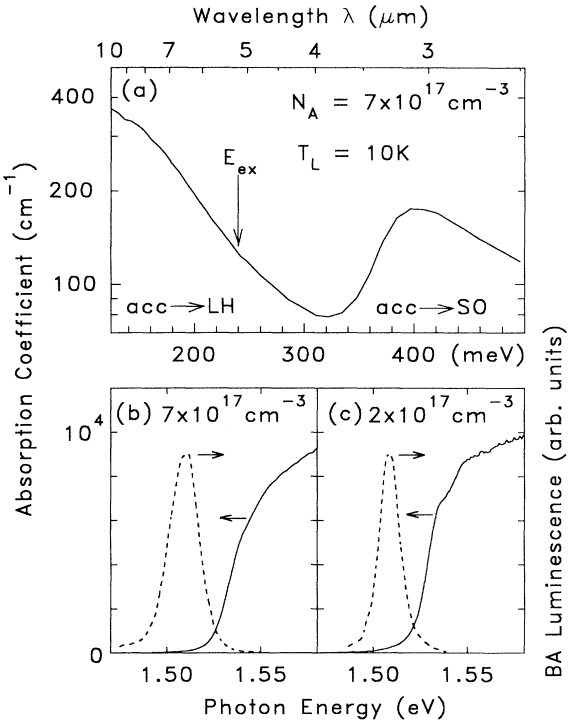

FIG. 2. (a) Midinfrared absorption spectrum of p-type GaAs for a lattice temperature of $T_L = 10$ K (acceptor concentration $N_A = 7\times10^{17}$ cm^{-3}). The two observed absorption bands are due to the photoionization of neutral acceptors into the light hole (acc.$\rightarrow$LH) (see Fig. 1) and split-off band (acc.$\rightarrow$SO). The spectral position of the picosecond excitation pulse is marked by the arrow E_{ex}. (b) Solid line: the absorption edge of p-type GaAs ($N_A = 7\times10^{17}$ cm^{-3}) at $T_L = 10$ K. Dashed curve: emission spectrum. The electrons recombine with holes bound to the acceptor ions [band-to-acceptor (BA) luminescence]. (c) Absorption edge and BA luminescence of a Zn-doped sample with a lower acceptor concentration of $N_A = 2.3\times10^{17}$ cm^{-3}.

The BA luminescence represents the counterpart to the acceptor deionization band which is used in our experiments as a probe of the acceptor ground-state population. The luminescence data give direct information on the strength and the shape of the acceptor deionization band as will be discussed in Sec. V B. The maximum of the luminescence spectrum around $E_{pr} \simeq 1.510$ eV indicates the onset of the deionization band. The latter continuously extends to higher photon energies due to allowed transitions to the continuum states of the conduction band (see Figs. 1 and 5).[23]

B. Time-resolved measurements

Transient absorption changes in the range of the acceptor deionization band of the two samples were monitored in spectrally and temporally resolved experiments. We first present results for the crystal with an acceptor concentration of $N_A = 7\times10^{17}$ cm^{-3}. In Fig. 3, data recorded at a lattice temperature of $T_L = 10$ K are presented for photon energies E_{pr} of the probe pulses of (a) 1.505, (b) 1.509, (c) 1.512, (d) 1.520, and (e) 1.531 eV. The photon energy of the excitation pulses was $E_{ex} = 240$ meV ($\lambda = 5.2$ μm) as indicated by the arrow in Fig. 2(a). The excitation density has a value of $N_{ex} \simeq 10^{17}$ cm^{-3}. On the left-hand side of Fig. 3, the induced absorption $\Delta A = -\ln(T/T_0)$ is plotted versus the delay time t_D between the excitation and probe pulses (points). T_0 and T represent, respectively, the transmission of the sample prior to and after excitation. The solid lines are the results of model calculations which will be discussed below.

Independent of the value of E_{pr}, we observe an increase of absorption ($\Delta A > 0$) within the time resolution of the experiment. The signal decays on a time scale of 100 ps following a nonexponential kinetics. At $E_{pr} = 1.520$ eV [Fig. 3(d)], the strongest absorption increase $\Delta A \simeq 0.7$ is observed that decays quite slowly towards the stationary absorption. Even at $t_D = 100$ ps a value of $\Delta A \simeq 0.1$ is measured. The maximum ΔA is smaller at frequencies below and above $E_{pr} = 1.520$ eV where shorter decay times of the signal are found. Within the experimental accuracy, data taken with a lower excitation density of $N_{ex} = 5\times10^{16}$ cm^{-3} exhibit the same kinetics at the different spectral positions E_{pr}.

On the right-hand side of Fig. 3, our data are replotted as $1/\Delta A$ versus t_D. In this representation, the data points follow a linear time dependence (solid lines), with a slope depending upon the probe energy E_{pr}. It is in-

teresting to note that the intersection of the straight lines with the abscissa occurs for all probe frequencies at a common value of $t_D \simeq -6$ ps. The linear relationship between $1/\Delta A$ and t_D corresponds to a $1/t_D$ behavior of ΔA.

Transient absorption changes were also studied with the sample of the lower acceptor concentration of $N_A = 2.3 \times 10^{17}$ cm^{-3}. The experimental results for four different probe energies are shown in Figs. 4(a)–4(d). The photon energy of the excitation pulses and the excitation density have values of $E_{ex} = 150$ meV and 10^{17} cm^{-3}, respectively. Qualitatively, we observe a similar temporal behavior of the induced absorption as for the sample with the higher doping concentration: The maximum value of ΔA and the slowest decay rate are observed at $E_{pr} = 1.520$ eV [Fig. 4(c)]. However, the overall relaxation rates found in this second sample are approximately twice the rates for the first crystal with $N_A = 7 \times 10^{17}$ cm^{-3}.

The spectral shape of the transient acceptor deionization band was derived from the time-resolved data of

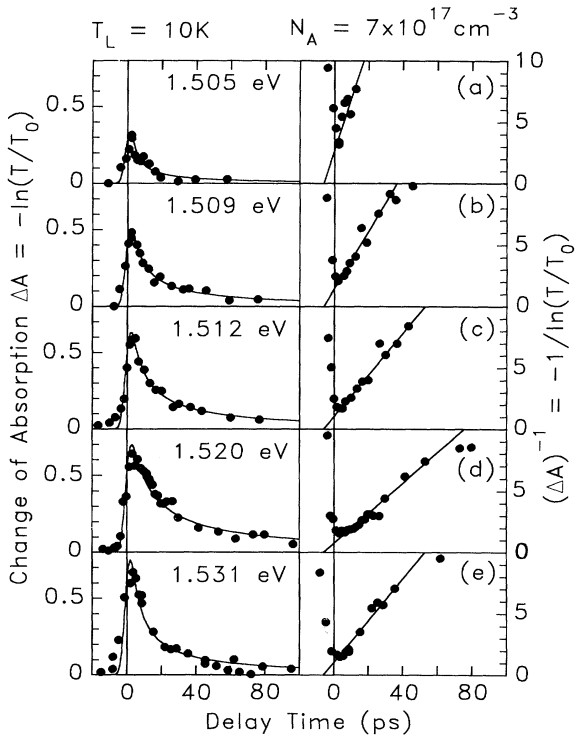

FIG. 3. Time-dependent change of absorption of the acceptor deionization band after picosecond infrared excitation at $E_{ex} = 240$ meV (lattice temperature $T_L = 10$ K). Left-hand side: the increase of absorption $\Delta A = -\ln(T/T_0)$ (solid circles) is plotted vs the delay time t_D between pump and probe pulses for probe energies E_{pr} of (a) 1.505, (b) 1.509, (c) 1.512, (d) 1.520, and (e) 1.531 eV (T_0, T: transmission of the sample prior to and after excitation, respectively). Right-hand side: The inverse signal $1/\Delta A$ shows a linear behavior as a function of the delay time with a slope depending on the specific value of E_{pr}. The solid lines are the results of model calculations.

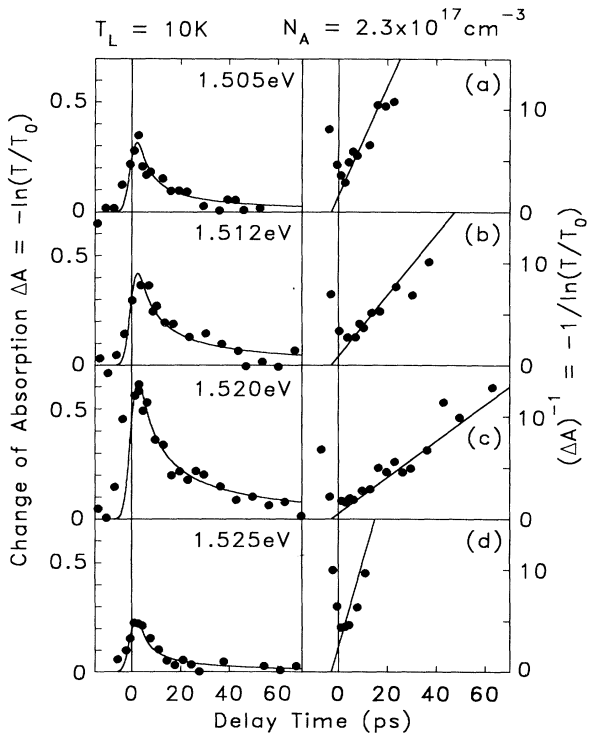

FIG. 4. Time-resolved data of the sample with a lower acceptor concentration of $N_A = 2.3 \times 10^{17}$ cm^{-3} for four different probe frequencies E_{pr} (lattice temperature $T_L = 10$ K). The photon energy of the excitation pulses amounts to $E_{ex} = 150$ meV.

Figs. 3 and 4. In Fig. 5, the induced absorption $\Delta A(E_{pr})$ of the two samples is plotted versus the photon energy E_{pr} for several fixed delay times (circles: 3 ps, diamonds: 10 ps; triangles: 40 ps, left-hand ordinate scale). The corresponding absorption coefficient $\alpha = \Delta A/(N_{A^-} l)$ calculated from the momentary density of ionized acceptors N_{A^-} and the sample thickness l is indicated on the right-hand side. The dashed lines which are in good agreement with the experimental data represent calculated deionization bands as will be discussed below. The stationary absorption spectra of the samples at $T_L = 10$ K (solid lines) are shown for comparison. The impurity-related absorption band rises close to the center of the band-to-acceptor luminescence [see Figs. 2(b) and 2(c)], reaches a broad maximum at about 1.530 eV, and slowly decreases towards higher energies. For probe energies $E_{pr} \geq 1.520$ eV, the acceptor deionization band overlaps substantially with the fundamental band-to-band absorption. Generation of free holes populating states close to the maximum of the valence bands leads to a decrease of the band-to-band absorption by band filling, i.e., an absorption change $\Delta A_{BF} < 0$. At $E_{pr} \geq 1.520$ eV, this transient bleaching as well as the increase of the impurity-related absorption contribute to the overall absorption change $\Delta A(E_{pr})$. As a result, the experimental points for this high E_{pr} value in Fig. 5 are below the calculated deionization band. We emphasize that the transient absorption

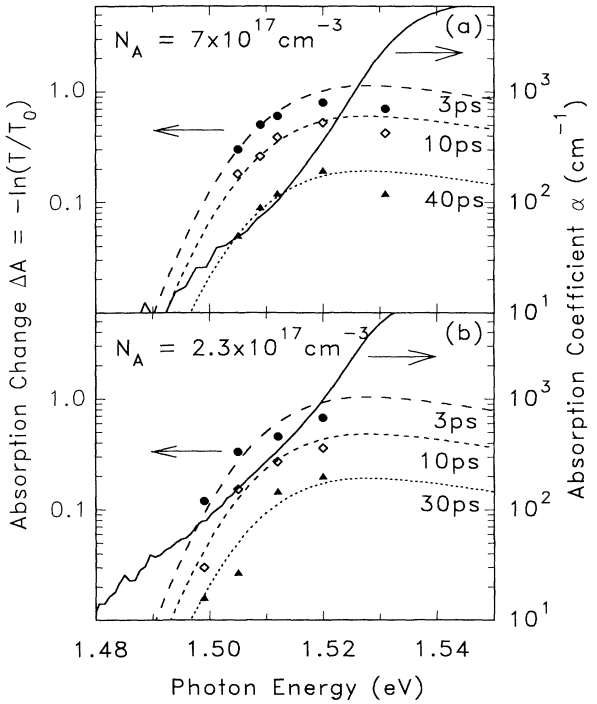

FIG. 5. (a) Transient acceptor deionization band ΔA vs photon energy for delay times t_D of 3 ps (solid circles), 10 ps (diamonds), and 40 ps (triangles), derived from the picosecond measurements of Fig. 3 ($N_A = 7\times10^{17}$ cm^{-3}, $T_L = 10$ K). Dashed lines: calculated frequency dependence of the transient absorption band. The measured absorption spectrum of the p-type GaAs sample is shown for comparison (solid line). (b) Time evolution of the deionization band for the sample with lower acceptor concentration of $N_A = 2.3\times10^{17}$ cm^{-3} (Fig. 4) at three different delay times t_D of 3, 10, and 30 ps.

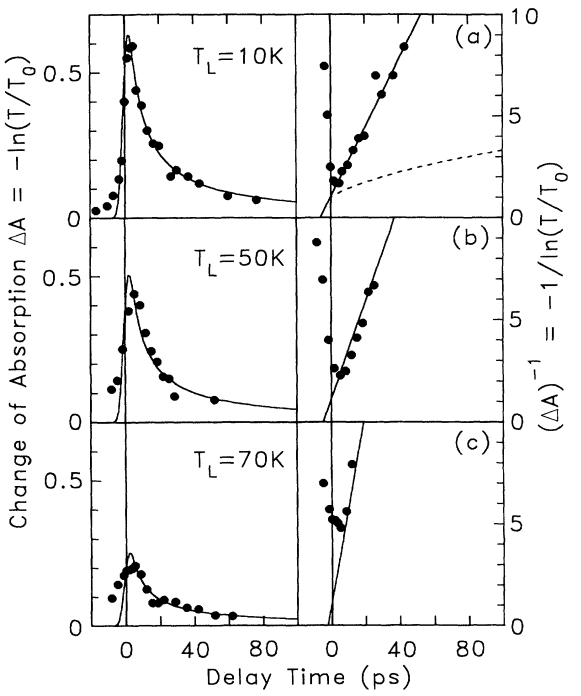

FIG. 6. Transient absorption change $\Delta A(t_D)$ vs delay time at $E_{pr} = 1.512$ eV for three different lattice temperatures T_L of (a) 10, (b) 50, and (c) 70 K (doping concentration $N_A = 7\times10^{17}$ cm^{-3}, excitation frequency $E_{ex} = 240$ meV). The dashed line in (a) represents the capture kinetics calculated from a theoretical model of Auger recombination.

band decays without changing its shape [dashed lines in Figs. 5(a) and 5(b)], i.e., the absorption change at different probe energies (see Figs. 3 and 4) reflects the *same* relaxation dynamics of the photoexcited carriers.

Additional time-resolved measurements were performed at higher lattice temperatures T_L. For the sample with $N_A = 7\times10^{17}$ cm^{-3}, the transient absorption change $\Delta A(t_D)$ at a probe frequency of $E_{pr} = 1.512$ eV is plotted in Fig. 6 for three different lattice temperatures of (a) 10, (b) 50, and (c) 70 K (excitation energy $E_{ex} = 240$ meV). We find again a linear relationship between the inverse absorption change $1/\Delta A$ and the delay time t_D. The smallest decay rate is observed for the lowest lattice temperature of $T_L = 10$ K. A similar behavior is noticed for the sample with the lower acceptor concentration of $N_A = 2.3\times10^{17}$ cm^{-3}.

IV. DISCUSSION

We now wish to discuss the different relaxation processes which the holes undergo after infrared excitation from the initially neutral acceptors to the light-hole band.

(i) Immediately after photoexcitation, the nonequilibrium distribution of holes transforms to a quasiequilibrium distribution in the delocalized continuum states of the HH and LH valence bands. Carrier-carrier scattering and the interaction of holes with optical phonons represent the most efficient scattering processes for this thermalization of the carrier distribution. Carrier-carrier scattering at densities between 10^{17} and 10^{18} cm^{-3} results in equilibration of the holes in each band within 100 fs as was found both experimentally[24,25] and in Monte Carlo simulations.[26,27] Inter-valence-band scattering via the polar-optical interaction and via the optical deformation potential occurs on a similar time scale. Both relaxation processes are completed well below one picosecond, i.e., within the time resolution of our present experiments.

(ii) The two scattering mechanisms mentioned in (i) result in a randomization of the excess energy supplied by the exciting infrared photon, i.e., a hot quasiequilibrium distribution with a temperature T_C higher than the lattice temperature ($T_C \gg T_L = 10$ K) is formed. Successive intraband emissions of LO and TO phonons transfer the excess energy rapidly to the lattice. Several time-resolved measurements on hole cooling in intrinsic and n-doped GaAs reveal very high-energy loss rates of several hundreds of meV/ps and a decrease of T_C from hundreds of kelvins to less than 50 K within the first 5 ps after excitation.[25,28–30] The remaining small excess energy of the carriers is transferred to the lattice predominantly by

emission of acoustic phonons, a relatively slow process that takes several hundred picoseconds.[31]

(iii) Finally, the photogenerated excess population of free holes decays by recombination with negatively charged acceptors. This last relaxation step is directly monitored in our measurements taking the strength of the deionization band as a measure of the momentary population of the acceptor ground state. The nonexponential decay of the transient absorption in Figs. 3, 4, and 6 that occurs on a time scale of several tens of picoseconds allows a quantitative analysis of the dynamics of hole capture.

Different possible capture mechanisms will be detailed in Sec. VI. In the following, we consider the overall capture rate in a quantitative way. The change of the density of free holes with time, dp/dt, is proportional to the density of free holes $p(t)$ and to the density of unoccupied acceptors $N_{A^-}(t)=p(t)$. This fact is expressed by the (nonlinear) differential equation for the time-dependent free hole density $p(t)$:

$$\frac{dp}{dt}=\frac{I_{\rm ex}(t)}{E_{\rm ex}}\sigma_{IR}(E_{\rm ex})(N_A-p)-C_{\rm trap}(T_C)p^2 + G_{\rm therm}(T_L)(N_A-p)\ . \quad (1)$$

The first term on the right-hand side of Eq. (1) describes the photoionization of the impurities where $N_{A^0}=N_A-p$ is the momentary density of neutral acceptors A^0, $I_{\rm ex}(t)$ is the time-dependent intensity of the excitation pulse, and $\sigma_{IR}(E_{\rm ex})$ represents the cross section of the acc.$\rightarrow$LH transition [see Fig. 2(a)]. The generation term is appreciable only during the 2-ps excitation pulse. The trapping rate of free holes is determined by the parameter $C_{\rm trap}(T_C)$ which depends on the distribution of holes in $\mathbf{k}$ space, i.e., for a quasiequilibrium distribution on the temperature of the free carriers T_C. It should be noted that $C_{\rm trap}$ is independent of the density of free holes $p(t)$ (see also Sec. VI B). The third term on the right-hand side of Eq. (1) represents the rate of thermal generation of free holes where neutral impurities are ionized by interaction with the optical-phonon bath of the crystal. (Acoustic phonons can be neglected because of the relatively large acceptor binding energy of 30 meV.) $G_{\rm therm}$ is proportional to the population of the optical-phonon branches; it can be neglected for the phonon populations occurring in our experiments at low lattice temperatures (see also Sec. VI C). Considering the time interval after the excitation pulse and assuming a constant carrier temperature T_C during hole capture [see (iii) above], Eq. (1) is solved by the expression

$$p(t)=\frac{1}{1/p_0+C_{\rm trap}t}\ , \quad (2)$$

where p_0 is the initially generated density of free holes at $t=0$. The measured change of absorption $\Delta A(E_{\rm pr},t)=-\ln(T/T_0)=p(t)\sigma_{\rm deion}(E_{\rm pr})l$ is proportional to $p(t)$, with the frequency-dependent cross section of the acceptor deionization band $\sigma_{\rm deion}(E_{\rm pr})$ and the sample thickness $l\simeq 10\ \mu$m. Correspondingly, the inverse absorption change $1/\Delta A$ obeys the equation

$$\frac{1}{\Delta A(t,E_{\rm pr})}=\frac{1}{p_0\sigma_{\rm deion}(E_{\rm pr})l}+\frac{C_{\rm trap}}{\sigma_{\rm deion}(E_{\rm pr})l}t\ . \quad (3)$$

This linear time behavior of $1/\Delta A$ with a slope depending on $C_{\rm trap}$ and the absorption cross section $\sigma_{\rm deion}(E_{\rm pr})$ is in accordance with our experimental findings. The solid lines in Figs. 3 and 4 are calculated from Eq. (3) with a single value of $C_{\rm trap}$ for each sample and with the frequency-dependent cross section $\sigma_{\rm deion}(E_{\rm pr})$ of the acceptor deionization band. The extrapolation of the calculated curves at different probe frequencies to $1/\Delta A(t_0,E_{\rm pr})=0$ gives a *common* intersection of $t_0=-(C_{\rm trap}p_0)^{-1}$. At $T_L=10$ K, we find $t_0=-6$ ps and -3 ps for the two samples with the higher (cf. Fig. 3) and the lower (cf. Fig. 4) acceptor concentration, respectively. With those numbers and with the initial hole density of $p_0\simeq 10^{17}$ cm^{-3}, one estimates $C_{\rm trap}\simeq(1.5\pm0.6)\times10^{-6}$ cm^3/s for the high acceptor concentration and $C_{\rm trap}\simeq(3.3\pm1.3)\times10^{-6}$ cm^3/s for the lower density of impurities. The experimental error is mainly determined by the uncertainties of the carrier concentration p_0 and by the accuracy of the zero point of the time scale (affecting t_0).

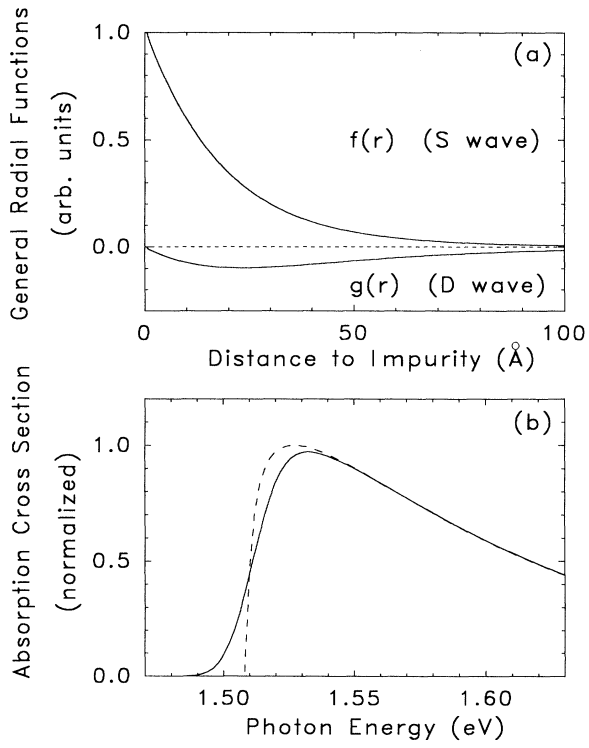

FIG. 7. (a) Calculated radial wave functions of shallow acceptor ground states in p-type GaAs are plotted vs the distance to the impurity center. $f(r)$ is the radial function of the S-wave symmetric part and $g(r)$ of the D-wave symmetric part of the effective mass impurity wave function. (b) Calculated absorption cross section of the acceptor deionization band as a function of photon energy (dashed line). The solid line represents the convolution of this spectrum with a Gaussian profile of a width of 19 meV accounting for the inhomogeneous broadening of the optical transition.

The absolute values of C_{trap} are derived with better accuracy from the slope of the inverse absorption change $d(\Delta A)^{-1}/dt$ and the frequency-dependent cross section of the deionization band $\sigma_{\text{deion}}(E_{\text{pr}})$ according to Eq. (3): $C_{\text{trap}}=[d(\Delta A)^{-1}/dt]\sigma_{\text{deion}}(E_{\text{pr}})l$. The absorption cross section $\sigma_{\text{deion}}(E_{\text{pr}})$ which will be discussed in detail in Sec. V B is plotted versus the photon energy E_{pr} in Fig. 7(b). The data taken at $T_L=10$ K give $C_{\text{trap}}=(1.5\pm0.3)\times10^{-6}$ and $(3.3\pm0.8)\times10^{-6}$ cm^3/s for the two samples with the higher (cf. Fig. 3) and the lower (cf. Fig. 4) acceptor concentration, respectively. For higher lattice temperatures (see Fig. 6), the deduced trapping parameters become distinctly larger. The results for different carrier temperatures T_C are summarized in Fig. 9 (solid circles: acceptor concentration $N_A=7\times10^{17}$ cm^{-3}; and open circles: $N_A=2.3\times10^{17}$ cm^{-3}). The capture rates will be analyzed and compared to model calculations (lines in Fig. 9) in Sec. VI.

V. QUANTITATIVE ANALYSIS

A. Acceptor wave function

The calculation of the optical dipole matrix elements and the scattering rates between delocalized states in the valence bands and the ground state of the acceptor requires a quantitative model for the acceptor wave function. Different to shallow donors in GaAs, the shallow Zn acceptors have a larger binding energy of $E_{\text{acc}}\simeq30$ meV (Ref. 16) and highly localized wave functions with an effective Bohr radius of the ground state of $a_B^*\simeq18$ Å. The geometrical size of the orbitals determines the volume of the acceptor levels in **k** space. A radius of $a_B^*=18$ Å corresponds to a broad wave-vector interval of $0\le k\le10^7$ cm^{-1}. As a result, **k** conservation is possible for coupling between continuum states within this wave-vector range and the acceptor ground state.

The diameter of the ground-state orbital of the Zn acceptor is large compared to the lattice constant of the GaAs crystal. Therefore the corresponding wave function can be derived with good accuracy in the effective mass approximation for the bound hole. Here the valence-band structure with two strongly warped (nonspherical) subbands (HH and LH) of different effective masses [$m_{\text{HH}}=0.56m_0$ and $m_{\text{LH}}=0.074m_0$ for GaAs (Ref. 32)] has to be taken into account. The calculations presented in the following are based on the formalism developed in Ref. 33. The most general acceptor Hamiltonian[34,35] consists of two terms: a first strictly spherical part and a second component comprising the cubic contributions (warping of the valence bands) as a perturbation. The impurity ground state is very well approximated by the spherical model.[33] The Hamiltonian can be thought of as describing a modified hydrogen atom perturbed by a "spin-orbit" interaction which couples the orbital and spin spaces to the total angular momentum $\mathbf{F}=\mathbf{L}+\mathbf{J}$ (the "spin" of the holes has a value of $J=\frac{3}{2}$ with $J_Z=\pm\frac{3}{2}$ in the case of heavy holes whereas $J_Z=\pm\frac{1}{2}$ for light holes). Accordingly, the acceptor states are classified following the L-S coupling scheme known for atomic systems. The wave function for the ground state of the acceptor is given by

$$\Phi(1S_{F=3/2})=f(r)Y_{00}(\theta,\phi)|J=\tfrac{3}{2},J_z=F_z\rangle+g(r)\sum_{L_z}Y_{2L_z}(\theta,\phi)C_{L_z,J_z,F,F_z}\times|J=\tfrac{3}{2},J_z=F_z-L_z\rangle\ . \tag{4}$$

$Y_{LM}(\theta,\phi)$ are the spherical harmonics, $C_{L_z,J_z,F,F_z}=\langle L=2,J=\frac{3}{2},L_z,J_z|J,L,F=\frac{3}{2},F_z\rangle$ are the Clebsch-Gordan coefficients, and $|J=\frac{3}{2},J_z\rangle$ represents the cell periodic parts of the wave function (contributions of the different valence bands HH and LH). The spin-orbit term couples only hydrogenic states for which $\Delta L=0,\pm2$ and, thus, the acceptor ground-state wave function consists of S-wave symmetric as well as D-wave symmetric functions. The corresponding general radial functions $f(r)$ (S wave) and $g(r)$ (D wave) have been calculated using the parameters for GaAs (Ref. 33) and are plotted as a function of the distance to the impurity center in Fig. 7(a). The main part of the effective mass acceptor wave function is S-wave symmetric [$f(r)$] and is very close to a $1S$ hydrogen wave function with an effective Bohr radius of $a_B^*=18$ Å.

B. Photodeionization of shallow acceptors

In our experiments, the deionization band of the acceptors serves as a probe of the momentary population of the acceptor ground state. The quantitative analysis of the trapping parameter C_{trap} introduced in Eq. (1) requires the absolute value of $\sigma_{\text{deion}}(E_{\text{pr}})$ at the different photon energies E_{pr} of the picosecond probe pulses. In the following, we determine the magnitude of $\sigma_{\text{deion}}(E_{\text{pr}})$.

(i) The *spectrally integrated* oscillator strength of the deionization band is derived from a measurement of the radiative lifetime τ_{BA} of the band-to-acceptor luminescence. This emission is the reverse process of the photodeionization of negatively charged impurities and is governed by the same matrix element [cf. Figs. 1, 2(b), and 2(c)]. The principle of detailed balance requires that the rate of radiative recombination at thermal equilibrium is equal to the corresponding rate of generation of electron-hole pairs via the same transition.[36] For transitions between the acceptor levels and the conduction band, the recombination rate $R^{\text{eq}}(T)$ and generation rate $G^{\text{eq}}(T)$ are given by

$$R^{\text{eq}}(T)=\frac{n^{\text{eq}}(T)}{\tau_{\text{BA}}(T)}=G^{\text{eq}}(T)=N_{A^-}^{\text{eq}}(T)\frac{1}{\pi^2\hbar^3}\left[\frac{n}{c}\right]^2\int_0^\infty\frac{d\hbar\omega(\hbar\omega)^2\sigma_{\text{deion}}(\hbar\omega)}{\exp(\hbar\omega/k_BT)-1}\ , \tag{5}$$

where $n^{\text{eq}}(T)$ and $N_{A^-}^{\text{eq}}(T)$ are the equilibrium densities of electrons and ionized acceptors, respectively. At low temperatures ($k_BT\ll E_{\text{acc}}$), only a small fraction of the

impurities are ionized and the equilibrium densities are calculated in Boltzmann approximation:

$$n^{eq}(T)=2\left[\frac{m_{CB}k_BT}{2\pi\hbar^2}\right]^{3/2}\exp\left[\frac{\mu-E_{gap}}{k_BT}\right], \quad (6)$$

$$p^{eq}(T)=2\left[\frac{m_{HH}k_BT}{2\pi\hbar^2}\right]^{3/2}\exp\left[\frac{-\mu}{k_BT}\right]$$

$$=N_A^{eq}(T)=\frac{N_A}{g_A\exp[(E_{acc}-\mu)/k_BT]-1}. \quad (7)$$

N_A is the total acceptor concentration and $g_A=4$ is the spin degeneracy of acceptor ground states $1S_{3/2}$ [see Eq. (4)]. The evaluation of Eq. (5) shows that the radiative lifetime of the BA luminescence τ_{BA} is nearly independent of the temperature T (for $T\ll 100$ K) and of the acceptor binding energy E_{acc}, but depends on the cross section of the deionization band $\sigma_{deion}(E_{pr})$. Thus a measurement of τ_{BA} gives quantitative information on $\sigma_{deion}(E_{pr})$. The radiative lifetime τ_{BA} was experimentally determined by measuring the quantum efficiency $\eta_{BA}=\tau_{lum}/\tau_{BA}$ and the luminescence decay time τ_{lum} with a calibrated luminescence detector and a picosecond streak camera system, respectively. We obtain a radiative lifetime of $\tau_{BA}=0.35$ ns for the sample with the higher doping concentration ($N_A=7\times10^{17}$ cm^{-3}) and $\tau_{BA}=1.13$ ns for the crystal with $N_A=2.3\times10^{17}$ cm^{-3}. Within the experimental accuracy, the ratio of two radiative lifetimes is equal to the ratio of the corresponding acceptor concentrations, as predicted by Eq. (5).

(ii) The *spectral envelope* of the deionization band was calculated within the theoretical framework developed in Refs. 1 and 37. The frequency-dependent absorption cross section $\sigma_{deion}(E_{pr})$ is given by

$$\sigma_{deion}(\hbar\omega)=\frac{C}{\omega}\sum_{\mathbf{k}}|M_{deion}(\mathbf{k})|^2\delta(E_{CB}(\mathbf{k})-E_{acc}-\hbar\omega). \quad (8)$$

$M_{deion}(\mathbf{k})$ represents the k-dependent dipole matrix element of the transition between the impurity level and the final state in the conduction band (Fig. 1). This quantity is related to the dipole matrix element $M_{CV}(\mathbf{k})$ of the band-to-band transition by

$$M_{deion}(\mathbf{k})=M_{CV}(\mathbf{k})\langle\Psi_f|\Psi_i\rangle,$$

where the second factor on the right-hand side represents the overlap integral of the effective mass envelope wave functions Ψ_i (acceptor) and Ψ_f (conduction band). In Refs. 1 and 37, $M_{CV}(\mathbf{k})$ is assumed to be constant and the overlap factor is calculated with a hydrogenlike Ψ_i and a plane wave Ψ_f. In our improved calculation, we introduce the k-dependent interband matrix element of Ref. 38 and the acceptor wave function of Eq. (4).[33] The normalized deionization band calculated in this way is plotted in Fig. 7(b) (dashed line). The spectrum starts at the center of the BA luminescence [Figs. 2(b) and 2(c)], reaches its maximum for a photon energy of $E_{pr}=1.53$ eV, and decreases slowly to higher photon energies. Equation (8) neglects mechanisms leading to a spectral broadening of the deionization band. Scattering processes due to carrier-carrier, carrier-impurity, and carrier-phonon interaction cause dephasing of the dipole transition (dephasing time T_2) resulting in a homogeneous broadening. In addition, the statistical fluctuations of the acceptor density in the GaAs crystal lead to changes of the overlap between the wave functions of neighboring impurities modifying the acceptor binding energies (inhomogeneous broadening). The overall broadening ΔE is estimated from the linewidth [full width at half maximum (FWHM)] of the BA luminescence which is subject to the same mechanisms. We obtain $\Delta E=19$ meV for the sample with $N_A=7\times10^{17}$ cm^{-3} and $\Delta E=13$ meV for $N_A=2.3\times10^{17}$ cm^{-3}. (The bandwidth of luminescence due to the finite width of the electron distribution in the conduction band is negligible compared to these values.) The solid line in Fig. 7(b) represents the convolution of the spectrum calculated from Eq. (8) (dashed line) with a Gaussian profile of $\Delta E_{FWHM}=19$ meV.

The normalized spectrum of Fig. 7(b) (solid line) was used in the integral of Eq. (5) to determine the absolute values of $\sigma_{deion}(E_{pr})$. For both samples, we obtain $\sigma_{deion}(1.53\text{ eV})=2.2\times10^{-14}$ cm^2 for the maximum of the deionization band at 1.53 eV.[39] For a density of ionized acceptors $N_A^-=5\times10^{16}$ cm^{-3}, one calculates an absorption coefficient $\alpha\simeq1000$ cm^{-1}.

VI. MECHANISMS OF HOT HOLE CAPTURE

Capture of free holes is equivalent to a transition of the carrier from continuum states to localized levels of the impurity atoms. For acceptor concentrations above 10^{17} cm^{-3}, high-lying levels of the impurity atoms show a substantial spatial overlap resulting in a delocalization of carriers. Consequently, those states are part of the (delocalized) continuum. In our present work, we concentrate on the repopulation of the acceptor *ground* state which is directly monitored via transient changes of the deionization band. In the microscopic capture process, the excess energy of the free hole relative to the impurity ground state is transferred to other free carriers or to the lattice. In addition to the total energy, the $\mathbf{k}$ vector must be conserved within the finite width of the impurity ground state in $\mathbf{k}$ space. Two types of mechanisms have to be distinguished. (i) Cascade-type trapping corresponds to a multiple-step relaxation where small amounts of energy (a few meV) are released by transitions from the continuum to the (closely spaced) excited levels of the acceptor atoms.[10] This type of trapping, which is mediated by carrier-carrier scattering or by acoustic-phonon emission, is important for the population of excited acceptor states. However, the transition rates are negligible for an energy separation of the levels involved that is larger than the average amount of transferred energy of several meV.[40] Consequently, cascade processes cannot account for the repopulation of the impurity ground state which—for Zn acceptors—is approximately 20 meV below the first excited state. (ii) Carrier capture is also possible by single-step transitions where the total amount of excess energy is transferred to a third (quasi)particle. In Fig. 8, three

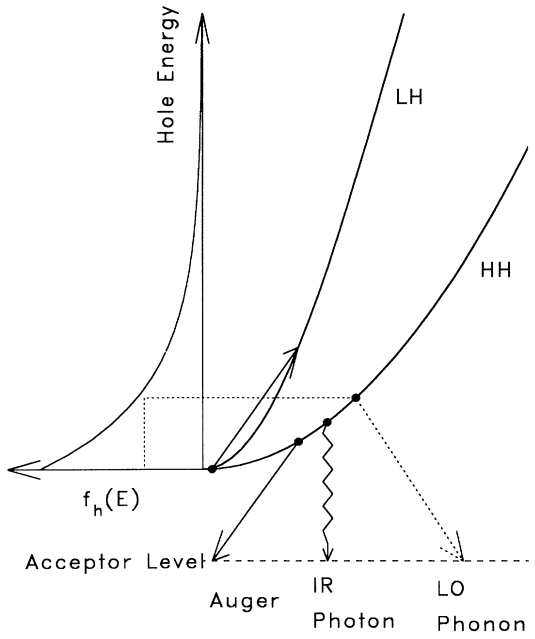

FIG. 8. Schematic of three single-step recombination mechanisms of free holes h with negatively charged acceptor ions Zn^- illustrated in a simplified valence-band structure of p-type GaAs: (a) solid arrows: Auger recombination; (b) zigzag arrow: radiative trapping; (c) dotted arrow: capture of free holes via emission of polar-optical phonons. Left-hand side: distribution function of free holes $f_h(E)$ in the valence bands HH and LH. The capture rate via LO-phonon emission depends on the occupation $f_h(E_h)$ of valence-band states with a hole energy of $E_h = E_{LO} - E_{acc}$.

possible mechanisms are depicted schematically: radiative recombination by emission of a far-infrared photon, Auger processes, and trapping by emission of single optical phonons. In the following paragraphs, the capture rates associated with these processes are analyzed quantitatively. We demonstrate that emission of optical phonons represents the dominant capture mechanism in our experiments.

A. Radiative trapping

The capture rate due to spontaneous emission of far-infrared photons is determined by the probability of radiative transitions to the acceptor ground state. The latter is proportional to the cross section σ_{photo} of the inverse process, the photoionization of neutral impurities [see also Fig. 2(a)]. Near the threshold of photoionization ($\hbar\omega \simeq E_{acc}$), σ_{photo} is estimated from the photoionization of a hydrogenlike system and is given by[17]

$$\sigma_{photo} = \frac{2^9\pi^2}{3\exp 4}\frac{e^2}{\hbar c}\frac{a_B^{*2}}{n} . \tag{9}$$

a_B^* is the effective Bohr radius of the impurity wave function and n is the refractive index of the host crystal. The trapping parameter C_{trap}^{rad} of radiative recombination is obtained according to the principle of detailed balance:[17]

$$C_{trap}^{rad} = 2\sigma_{photo}\left[\frac{n\hbar\omega}{m_{HH}c}\right]^2\langle v_h^{-1}\rangle . \tag{10}$$

m_h^* represents the effective mass of the holes; $\langle v_h^{-1}\rangle$ is the inverse hole velocity averaged over the distribution function of free holes. It should be noted that this process favors the capture of low-velocity, i.e., cold carriers. For $\hbar\omega = E_{acc}$ and $T_C = 50$ K one estimates $C_{trap}^{rad} = 5\times10^{-13}$ cm^3/s. This value is several orders of magnitude smaller than the experimental C_{trap}. We conclude that—with radiative trapping being negligible—nonradiative processes dominate the capture dynamics observed in our measurements.

The capture of holes via emission of plasmons is also negligible in our experiments. Even for ionization of all impurities in the sample ($p = 7\times10^{17}$ cm^{-3}), the plasmon energy $\hbar\omega_{plasma} \simeq 10$ meV is significantly less than the acceptor binding energy $E_{acc} \simeq 30$ meV.

B. Auger recombination and impact ionization

The excess energy of the hole to be trapped can be transferred to another free hole that is promoted to a valence-band state of higher energy. The Auger capture rate W_{Auger} is proportional to the concentration of vacant impurities N_{A^-} and to the density of free holes $p(t) = N_{A^-}(t)$. Considering the time interval after the excitation pulse, we obtain the differential equation[17,41]

$$\left[\frac{dp}{dt}\right]_{Auger} = -W_{Auger}p = -\Lambda_{Auger}p^3 , \tag{11}$$

where the density-independent trapping parameter Λ_{Auger} is introduced. Equation (11) has the solution

$$p(t) = \left[\frac{1}{p_0^{-2} + \Lambda_{Auger}t}\right]^{1/2} , \tag{12}$$

which differs markedly from the $1/t$ behavior of Eq. (2).

A crude estimate of the Auger parameters Λ_{Auger} which significantly overestimates the Auger rates has been presented in Refs. 17 and 41:

$$\Lambda_{Auger} = \frac{e^4}{\hbar^3}\frac{m_h^*(4\pi a_B^{*2})^3}{\epsilon^2} . \tag{13}$$

Using the relevant parameters for p-type GaAs ($m_h^* = m_{HH}$, $\epsilon = 12.6$, and $a_B^* = 18$ Å) in Eq. (13), one estimates $\Lambda_{Auger} = 10^{-23}$ cm^6/s for the capture of heavy holes. The dashed line in Fig. 6(a) represents the inverse absorption change $1/\Delta A(t) = 1/[p(t)\sigma_{deion}(E_{pr})l]$ as calculated with the help of Eqs. (12) and (13) with $p_0 = 10^{17}$ cm^{-3}. A comparison between the calculated dashed line and the data points shows that Auger recombination is not the relevant trapping process in our investigation. The slope of the calculated curve decreases substantially at later delay times, a behavior not found in the experiment. Furthermore, the p^2 dependence of the Auger rate W_{Auger} predicts a strong change of the carrier dynamics with excitation density. Our data taken with reduced excitation density ($p_0 = 5\times10^{16}$ cm^{-3}), however, exhibit the

same kinetics of ΔA as the measurements for higher densities. The capture of holes via Auger processes is partly compensated for by impact ionization of neutral acceptors. Inelastic collisions of photoexcited holes of an energy $E_h > E_{acc}$ with neutral acceptors promote bound holes to continuum states. Significant rates of impact ionization only occur for large densities of free holes $p \geq 5\times 10^{16}$ cm^{-3}, a situation which barely exists during the picosecond excitation pulse. Thus impact ionization of neutral impurities might play a limited role during the excitation pulse of 2 ps duration, but can be neglected at delay times longer than 5 ps.

C. Hot hole capture via emission of optical phonons

The energy of transversal- ($\hbar\omega_{TO}=34$ meV) and of longitudinal-optical phonons ($\hbar\omega_{LO}=37$ meV) exceeds the ionization energy $E_{acc}\simeq 30$ meV of the Zn acceptors.[16] Thus transitions between delocalized states in the continuum and the impurity ground state are possible by absorbing (ionization) or emitting (capture) single optical phonons (OP). The capture rate is determined by the strength of carrier–optical-phonon coupling and by the population of the continuum states lying one phonon energy above the impurity ground state. The latter is depicted schematically by the Boltzmann tail on the left-hand side of Fig. 8. For a thermalized carrier distribution—as in our picosecond experiments—the hole population is determined by the carrier temperature. The strength of the hole-phonon (ep) interaction is given by[17]

$$|\langle f|H_{ep}|i\rangle|^2 = C(q)[n_{OP}(q)+\tfrac{1}{2}\pm\tfrac{1}{2}]I^2(f,i)|G(\mathbf{q},\mathbf{k})|^2 \ . \tag{14}$$

The matrix element on the left-hand side is taken between the initial continuum state i and the final acceptor ground state f. $C(q)$ represents the coupling strength between the carriers and the optical phonons which comprises the polar-optical interaction [Eq. (15)] and the deformation potential [Eq. (16)] (Ref. 17):

$$C_{pol}(q)=\frac{2\pi e^2\hbar\omega_{LO}}{V}\left[\frac{1}{\epsilon_\infty}-\frac{1}{\epsilon_s}\right]\frac{1}{q^2}\frac{q^4}{(q^2+q_0^2)^2} \ , \tag{15}$$

$$C_{def}(q)=\frac{D_{OP}^2\hbar}{2\rho V\omega_{OP}} \ . \tag{16}$$

ϵ_∞ and ϵ_s are the high-frequency and static dielectric constants of GaAs, respectively. The polar-optical coupling shows a $1/q^2$ dependence (q: phonon wave vector), modified by the last term of Eq. (15) which accounts for screening (q_0: screening vector). In the case of polar-optical scattering [Eq. (15)] the holes only interact with LO phonons, whereas both LO and TO phonons are involved in scattering processes via the deformation potential D_{OP} [Eq. (16)].

The respective phonon emission and absorption rates are proportional to $[n_{OP}(q)+1]$ and $n_{OP}(q)$, where $n_{OP}(q)$ represents the occupation probability of phonon states at the wave vector q. The equilibrium population of the optical-phonon branches is given by the Bose-Einstein expression $n_{OP}(q)=[\exp(\hbar\omega_{LO,TO}/kT_L)-1]^{-1}$. For a lattice temperature of $T_L=10$ K, $n_{OP}(q)\ll 1$, i.e., the rate of phonon absorption (impurity ionization) is negligible compared to the capture rate.

The quantity $I^2(f,i)$ in Eq. (14) is the square of the overlap integral between the periodic parts of the final (f) and the initial (i) wave function. The last term in Eq. (14) corresponds to the squared overlap integral of the slowly varying envelope parts $\Psi_f(\mathbf{r})$ and $\Psi_i(\mathbf{r})$ (effective mass approximation) and the phonon wave function $\exp(i\mathbf{qr})$:[42]

$$G(\mathbf{q},\mathbf{k})=\int dV\,\Psi_f^*(\mathbf{r})\exp(i\mathbf{qr})\Psi_i(\mathbf{r}) \ . \tag{17}$$

The initial wave function $\Psi_i(\mathbf{r})$ is a delocalized plane wave in one of the valence bands (HH or LH) which can be expanded into a series of functions each having a different angular momentum of orbital motion:

$$\Psi_i(\mathbf{r})=\frac{1}{\sqrt{V}}\exp(ikz)$$
$$=\frac{1}{\sqrt{V}}\sum_{L=0}^{\infty} i^L\sqrt{4\pi(2L+1)}\,j_L(kr)Y_{L0}(\theta,\phi) \ . \tag{18}$$

The radial functions $j_L(kr)$ are the spherical Bessel functions of the order L and $Y_{L0}(\theta,\phi)$ are the spherical harmonics. The final wave function $\Psi_f(\mathbf{r})$ is the localized ground-state orbital given by Eq. (4). The overlap function $G(\mathbf{q},\mathbf{k})$ which is obtained with those wave functions allows us to calculate the energy-dependent capture rate $W(E_h)$ with the help of Fermi's "golden rule" including both polar-optical and deformation potential scattering:

$$W(E_h)=\frac{2\pi}{\hbar}N_{A^-}\sum_{F_z}\frac{V}{(2\pi)^3}\int d^3\mathbf{q}|\langle f|H_{ep}|i\rangle|^2$$
$$\times\delta(E_h-E_{acc}-\hbar\omega_{OP}) \ . \tag{19}$$

The sum in Eq. (19) runs over all possible final states, i.e., the different degenerate states of the acceptor ground level E_{acc} labeled by quantum number F_z [see Eq. (4)] and the integral extends over the optical phonons with different wave vectors $\mathbf{q}$. The δ function in the integral assures energy conservation, i.e., only holes with a kinetic energy of $E_h=\hbar\omega_{OP}-E_{acc}$ undergo a transition to the acceptor ground state. The capture rate $W(E_h)$ is proportional to the concentration of ionized impurities N_{A^-}.

The trapping parameter C_{trap}^{OP} is calculated by averaging the capture rate $W(E_h)$ of Eq. (19) over the temperature-dependent distribution function $f_h(E_h,T_C)$ of free holes in the HH and LH bands:

$$C_{trap}^{OP}(T_C)$$
$$=\frac{1}{pN_{A^-}}\sum_{HH,LH}\int_0^\infty dE_h D(E_h)f_h(E_h,T_C)W(E_h) \ . \tag{20}$$

In Fig. 9, different curves of $C_{trap}^{OP}(T_C)$ calculated from Eq. (20) are plotted as a function of carrier temperature

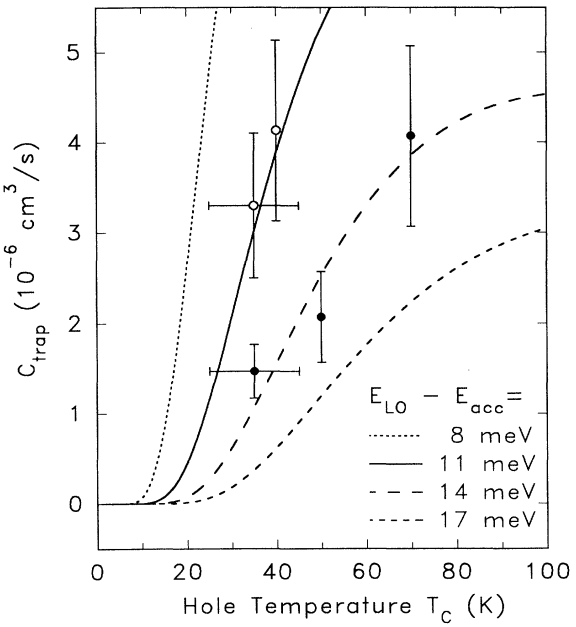

FIG. 9. Trapping parameter C_{trap}^{OP} calculated for hole trapping via emission of optical phonons as a function of the temperature of free holes (lines). C_{trap}^{OP} is plotted for three different hole energies E_h above the minimum of the continuum states $E_h = E_{LO} - E_{acc}$ (energy of the LO phonon $E_{LO} = 37$ meV). The symbols give the values of C_{trap} deduced from the time-resolved experiments at different lattice temperatures T_L for $N_A = 2.3 \times 10^{17}$ (open circles) and 7×10^{17} cm^{-3} (solid circles, Fig. 6), respectively.

T_C for several values of $E_{LO} - E_{acc}$ (with $E_{LO} = 37$ meV). The capture parameter increases strongly with temperature because of the larger population of the relevant states in the valence bands. C_{trap}^{OP} depends markedly on $\Delta E = E_{LO} - E_{acc}$. For large values of ΔE, hole capture originates from higher-lying states in the valence bands where a smaller population gives rise to a reduced value of C_{trap}^{OP}. The absolute values of C_{trap}^{OP} are in the range of several 10^{-6} cm^3/s resulting in capture rates $W_{trap}(T_C) = C_{trap}^{OP} p$ of several 10^{10} s^{-1} for a hole density of $p_0 = 10^{17}$ cm^{-3}. A more detailed inspection shows that those high trapping rates are mainly due to the polar-optical interaction favoring the emission of phonons with small wave vectors q. The q-independent deformation potential contributes only 10% to the overall capture rate.

The trapping rates calculated for optical-phonon emission compare very well with our experimental results, reproducing the correct order of magnitude of C_{trap}. We conclude that emission of single optical phonons represents the main mechanism of hole capture on a time scale of several tens of picoseconds. In Fig. 9, experimental data for the two samples with higher (points) and lower doping concentration (open circles) are directly compared with the calculated curves. For a lattice temperature $T_L \geq 40$ K, the carrier temperature T_C is practically equal to T_L. At $T_L = 10$ K, the holes remain at $T_C > T_L$ because of the slowing down of intraband cooling by emission of optical phonons. We estimate an approximate value of $T_C \simeq 35$ K during the time interval over which capture occurs (see also Sec. IV). The trapping parameters derived for the sample with higher doping concentration (solid circles) are close to the curve calculated for $E_{LO} - E_{acc} = 14$ meV corresponding to $E_{acc} = 23$ meV, whereas the higher trapping rates for the lower acceptor density (open circles) are better reproduced by the calculation with $E_{LO} - E_{acc} = 11$ meV, i.e., $E_{acc} = 26$ meV. Those E_{acc} values are somewhat smaller than the ionization energy $E_{acc} \simeq 30$ meV which was determined by infrared studies of samples with a very low (net) p doping below 10^{15} cm^{-3}, i.e., fully isolated acceptors.[16] This observation is rationalized as follows. In our samples with a doping concentration higher than 10^{17} cm^{-3}, the impurities start to interact with each other because of their smaller mean distance and/or statistical fluctuations of the acceptor density. Due to the latter, a certain fraction of impurities show a mutual separation which is less than the mean distance, and thus an even stronger interaction. This coupling leads to a broadening of the impurity levels and to the well-known decrease of the ionization energy with increasing concentration,[43] changing the overall trapping rates because of their dependence on $E_{LO} - E_{acc}$.

A final comment should be made on excess populations of optical phonons. In our experiments, two generation mechanisms of excess phonons have to be considered. (i) Infrared photoexcitation supplies an excess energy of roughly 200 meV per excited hole. After thermalization to the heavy-hole band within less than 1 ps, the hot hole distribution cools down predominantly by emission of LO and TO phonons. These phonons emitted via intraband scattering cover a very broad wave-vector interval of several 10^7 cm^{-1} due to the weak k dispersion of the heavy-hole band (large heavy-hole mass). Considering the time and wave-vector-dependent phonon emission rates[44] one estimates a maximum population of the optical-phonon branches of $n_{OP}(q) \leq 0.01$. (ii) Trapping of the free holes by the ionized acceptors also creates optical phonons. The generation rate of these phonons has a value of several 0.01 ps^{-1}, as calculated from Eq. (20). This number is considerably smaller than the phonon decay rate of 0.14 ps^{-1} determined by the phonon lifetime of $\tau \simeq 7$ ps.[45] From those rates and from the maximum density $N_q \simeq p_0 = 10^{17}$ cm^{-3} of phonons that are emitted during carrier relaxation over a wave-vector interval of $k \simeq 10^7$ cm^{-1} one derives a phonon excess population even smaller than generated by carrier cooling. Consequently, the capture rates are practically unaffected by excess populations of LO and TO phonons.

VII. SUMMARY

In conclusion, the experimental results presented here give direct evidence of picosecond hole capture by shallow acceptors in p-type GaAs. Spectrally and time-resolved measurements using picosecond infrared pulses

were reported for two different doping levels of 2.3×10^{17} and 7×10^{17} cm^{-3}. In both cases, we find a repopulation of the acceptor ground state on a time scale of 10^{-11} s. Detailed quantitative calculations of carrier trapping rates comparing multiple-step and single-step capture processes demonstrate that emission of single optical phonons by hot holes via the polar-optical interaction represents the main mechanism of hole capture. In the present work, relaxation processes of free holes were monitored on a picosecond time scale. Future experiments with subpicosecond infrared pulses will give direct access to the carrier dynamics during the first picosecond after excitation where thermalization, carrier cooling, and trapping occur simultaneously. Those measurements are expected to extend our knowledge on ultrafast carrier trapping which is important for hot carrier transport as well as for the kinetics of impurity-related optical transitions in III-V semiconductors.

[1]W. P. Dumke, Phys. Rev. **132**, 1988 (1963).

[2]For a review see L. Reggiani and V. Mitin, Riv. Nuovo Cimento **12**, 1 (1989).

[3]A van der Ziel, *Noise: Source, Characterization, Measurement* (Prentice-Hall, Englewood Cliffs, NJ, 1970).

[4]L. Reggiani, P. Lugli, and V. Mitin, Appl. Phys. Lett. **51**, 925 (1987).

[5]V. L. Bonch-Bruevich and E. G. Landsberg, Phys. Status Solidi **29**, 9 (1968).

[6]For a review see V. N. Abakumov, V. I. Perel, and I. N. Yassievich, Fiz. Tekh. Poluprovodn. **12**, 5 (1978) [Sov. Phys. Semicond. **12**, 1 (1978)].

[7]S. H. Koenig, Phys. Rev. **110**, 986 (1958).

[8]E. E. Godik, Yu. A. Kuritsyn, and V. P. Sinis, Fiz. Tekh. Poluprovodn. **12**, 91 (1978) [Sov. Phys. Semicond. **12**, 51 (1978)].

[9]D. Bimberg, H. Münzel, A. Steckenborn, and J. Christen, Phys. Rev. B **31**, 7788 (1985).

[10]M. Lax, Phys. Rev. **119**, 1502 (1960).

[11]L. Reggiani, L. Varani, V. Mitin, and C. VanVliet, Phys. Rev. Lett. **63**, 1094 (1989).

[12]R. Ulbrich, Phys. Rev. Lett. **27**, 1512 (1971).

[13]M. Asche, H. Kostial, and O. G. Sarbey, Phys. Status Solidi B **91**, 521 (1979).

[14]O. G. Sarbey and M. Asche, Pis'ma Zh. Eksp. Teor. Fiz. **28**, 625 (1978) [JETP Lett. **28**, 578 (1978)].

[15]A. Lohner, M. Woerner, T. Elsaesser, and W. Kaiser, Phys. Rev. Lett. **68**, 3920 (1992).

[16]R. F. Kirkman, R. Stradling, and P. J. Lin-Chung, J. Phys. C **11**, 419 (1978).

[17]B. K. Ridley, *Quantum Processes in Semiconductors* (Clarendon, Oxford, 1982).

[18]T. Elsaesser, H. J. Polland, A. Seilmeier, and W. Kaiser, IEEE J. Quantum Electron. **QE-20**, 191 (1984).

[19]T. Elsaesser, H. Lobentanzer, and A. Seilmeier, Opt. Commun. **52**, 355 (1985).

[20]A. Penzkofer and W. Kaiser, Opt. Quantum Electron. **9**, 315 (1977).

[21]R. Braunstein and E. O. Kane, J. Phys. Chem. Solids **23**, 1423 (1962).

[22]E. J. Mayer, A. Lohner, M. Woerner, and T. Elsaesser, Phys. Rev. B **46**, 1878 (1992).

[23]The interband absorption and emission spectra as well as the deionization band are blueshifted by approximately 15 meV due to small strain in the thin GaAs crystals at low temperatures.

[24]T. Elsaesser, J. Shah, L. Rota, and P. Lugli, Phys. Rev. Lett. **66**, 1757 (1991).

[25]X. Q. Zhou, K. Leo, and H. Kurz, Phys. Rev. B **45**, 3886 (1992).

[26]L. Rota, P. Lugli, T. Elsaesser, and J. Shah, Phys. Rev. B **47**, 4226 (1993).

[27]M. J. Kann, A. M. Kriman, and D. K. Ferry, Phys. Rev. B **41**, 12 659 (1990).

[28]R. F. Leheny, J. Shah, R. L. Fork, C. V. Shank, and A. Migus, Solid State Commun. **31**, 809 (1979).

[29]W. Z. Lin, R. W. Schoenlein, J. G. Fujimoto, and E. P. Ippen, IEEE J. Quantum Electron. **QE-24**, 267 (1988).

[30]C. V. Shank, R. L. Fork, R. F. Leheny, and J. Shah, Phys. Rev. Lett. **42**, 112 (1979).

[31]K. Leo, W. W. Rühle, H. J. Queisser, and K. Ploog, Phys. Rev. B **37**, 7121 (1988).

[32]P. Lawaetz, Phys. Rev. B **4**, 3460 (1971).

[33]A. Baldereschi and N. O. Lipari, Phys. Rev. B **9**, 1525 (1974).

[34]J. M. Luttinger and W. Kohn, Phys. Rev. **97**, 869 (1955).

[35]J. M. Luttinger, Phys. Rev. **102**, 1030 (1956).

[36]W. van Roosbroeck and W. Shockley, Phys. Rev. **94**, 1558 (1954).

[37]D. M. Eagles, J. Phys. Chem. Solids **16**, 76 (1960).

[38]E. O. Kane, J. Phys. Chem. Solids **1**, 82 (1956).

[39]The absolute σ_{deion} (1.53 eV) calculated directly from Eq. (8) amounts to approximately 40% of this value. This discrepancy is mainly due to the fact that Coulomb enhancement of the band-to-band transitions is neglected in the calculation of the dipole matrix element $M_{CV}(\mathbf{k})$ which accounts only for 40% of the real absorption of GaAs.

[40]The relevant acoustic phonons have wave vectors $q < k_{\max} \simeq 10^7$ cm^{-1}, where $k_{\max}$ gives the extension of the impurity ground state in $\mathbf{k}$ space. The maximum energy of acoustic phonons $E_{\text{acoustic}} = \hbar v_s q$ (v_s: velocity of sound) has a value of 3 meV which is much smaller than the energy separation between the acceptor ground state and the first excited state.

[41]P. T. Landsberg, C. Rhys-Roberts, and P. Lal, Proc. Soc. London **84**, 915 (1964).

[42]F. A. Riddoch and B. K. Ridley, J. Phys. C **16**, 6971 (1983).

[43]N. F. Mott, Proc. R. Soc. London, Ser. A **382**, 1 (1982).

[44]W. Pötz and P. Kocevar, Phys. Rev. B **28**, 7040 (1983).

[45]D. von der Linde, J. Kuhl, and H. Klingenberg, Phys. Rev. Lett. **44**, 1505 (1980).